Revista Mexicana de Astronomía y Astrofísica, **40**, 61–67 (2004)

HERBIG-HARO JETS FROM SOURCES IN ELLIPTICAL ORBITS

R. F. González and A. C. Raga

Instituto de Ciencias Nucleares
Universidad Nacional Autónoma de México

Received 2003 November 27; accepted 2004 January 30

RESUMEN

En este trabajo, estudiamos la evolución cinemática de un flujo HH (Herbig-Haro) producido en un sistema estelar binario donde la fuente del chorro describe órbitas elípticas alrededor de la estrella compañera. Presentamos un modelo analítico que permite calcular la trayectoria de un chorro estelar balístico, y mostramos las diversas morfologías obtenidas para diferentes excentricidades del movimiento orbital. Adicionalmente, hemos calculado simulaciones hidrodinámicas en 3D de un chorro radiativo proveniente de una fuente estelar que se mueve en una órbita elíptica muy excéntrica. Efectuando una comparación de las simulaciones numéricas con el modelo analítico, mostramos que las diferencias principales entre ellos ocurre en la cabeza del chorro y en las zonas en que el haz del chorro tiene desviaciones máximas del eje orbital, debido a la interacción entre el chorro y el medio ambiente. Finalmente, presentamos los mapas de intensidad en Hα predichos por nuestras simulaciones numéricas, y mencionamos las propiedades observacionales esperadas para objetos HH expulsados por estrellas en órbitas elípticas.

ABSTRACT

In this paper, we study the kinematical evolution of a HH (Herbig-Haro) jet produced in a binary stellar system in which the jet source is moving in an elliptical orbit around a stellar companion. An anlytical model describing the motion of a ballistic jet is presented, showing diverse morphologies obtained for different ellipticities of the orbital motion. In addition, we have carried out a 3D hydrodynamical simulation of a radiative jet from a stellar source moving along a high-ellipticiy orbit. A comparison between the numerical simulations and the analytical model shows that the main deviations between them occur in the leading bow-shock and in the regions in which the jet beam has its larger deviations from the orbital axis, as a result of the interaction between the jet and the environment. Finally, we present the Hα intensity maps predicted from our numerical simulation, and discuss the observational properties expected for HH objects ejected from stars in elliptical orbits.

Key Words: **ISM: HERBIG-HARO OBJECTS — ISM: JETS AND OUTFLOWS — ISM: KINEMATICS AND DYNAMICS**

1. INTRODUCTION

Reipurth (2000) suggested that the sources of HH jets belong to binary (or multiple) systems, and that the interactions between the jet source and its stellar companions might be responsible for producing at least some of the structures observed along the jets themselves. This suggestion leads to several possible theoretical problems that deserve to be studied.

As discussed by Reipurth (2000), an important problem in this context are the possible perturbations of the jet production mechanism by the passage of a stellar companion in an elliptical orbit (which could in principle lead to a periodic or quasi-periodic variability of the ejection). Such effects, however, are difficult to study, in particular because the precise nature of the ejection mechanism is currently still uncertain (see, e.g., the review of Ferreira 2002).

An effect easier to study is the possible existence of a precession of the accretion disk around the jet source (due to the presence of a companion star in

a non-coplanar orbit), which could in turn cause a precession of the outflow axis. Terquem et al. (1999) have studied such a precession of an accretion disk, and suggested that the effect of this "disk precession" might be observed along some HH jets. Also, there are several papers which study analytic (Raga, Cantó, & Biro 1993) and numerical (Völker et al. 1999; Masciadri et al. 2002) models of the dynamics of jets with a precessing outflow axis, and compare the obtained structures with observations of HH jets.

Masciadri & Raga (2002) pointed out that a possibly more important effect in an outflow source with stellar companions is brought about by the fact that the source itself describes an orbital motion. In particular, since the orbital periods are shorter by a factor of ~ 10 than the period of the precession induced on an accretion disk (Terquem et al. 1999), the effect of the orbital motion is likely to be visible at shorter distances along the jet than the effect of the precession.

Masciadri & Raga (2002) derived an analytic (ballistic) model for a jet ejected from a source which is moving in a circular orbit, and compared the results of this model with observations of HH jets, and also with a 3D numerical simulation. In the present paper we extend this work to the more general case of a source moving in an elliptical orbit. As this problem has not been studied before, and because the number of free parameters of the problem (mostly unconstrained by observations) is quite large, we restrict ourselves to the case of jets with axes perpendicular to the orbital plane of the source.

In § 2, we derive an analytic (ballistic) solution for the motion of the jet, and show the diverse morphologies that can be obtained for orbits with different eccentricities. In § 3, we choose one particular set of parameters, and compute a 3D, radiative jet simulation, which we then compare with the analytic model. Finally, in § 4 we present a qualitative discussion of the observational properties expected for jets ejected from sources moving in elliptical orbits.

2. BALLISTIC MODEL

Let us consider a hypersonic HH jet ejected from a star moving in an elliptical orbit with major semiaxis a, eccentricity e, and angular frequency ω. For elliptic motion, the position r of the star (measured from one of the focci of the ellipse) is given by,

$$r = \frac{a(1-e^2)}{1+e\ \cos\theta}, \tag{1}$$

where θ is the polar angle. By convention, we have selected $\theta = 0$ at the periastron. In order to describe the motion of the star for elliptical orbits, it is more convenient to use the so-called eccentric anomaly ψ (see Goldstein 1980), which is defined by the equation

$$r = a(1 - e\ \cos\psi), \tag{2}$$

where ψ: $0 \rightarrow 2\pi$. The variable ψ is related to the time τ by Kepler's equation

$$\omega\tau = \psi - e\ \sin\psi, \tag{3}$$

and to the polar angle by

$$\tan\frac{\theta}{2} = \left(\frac{1+e}{1-e}\right)^{1/2} \tan\frac{\psi}{2}. \tag{4}$$

First, we compute ψ as a function of τ by numerically inverting Eq. (3), and we can then obtain r and θ (or $x = r\cos\theta$ and $y = r\sin\theta$) as a function of τ from Eqs. (2) and (4).

We now assume that the orbital axis (z) and the jet axis are parallel. Then, the components of the ejection velocity of the jet are given by

$$v_x = \dot{r}\ \cos\theta - r\dot{\theta}\ \sin\theta,$$

$$v_y = \dot{r}\ \sin\theta + r\dot{\theta}\ \cos\theta,$$

$$v_z = v_j, \tag{5}$$

where $\dot{r} = dr/d\tau$, $\dot{\theta} = d\theta/d\tau$ and v_j is the ejection velocity of the jet from the star (which we assume to be time-independent). From Eqs. (1)–(4), it follows that

$$\dot{r} = \frac{a\ e\ \sin\theta\ (1-e^2)}{(1+e\ \cos\theta)^2}\ \dot{\theta}, \tag{6}$$

$$\dot{\theta} = \left(\frac{1+e}{1-e}\right)^{1/2} \left[\frac{\cos(\theta/2)}{\cos(\psi/2)}\right]^2 \frac{\omega}{1-e\ \cos\psi}. \tag{7}$$

Therefore, the fluid parcel ejected from the star at a time τ, when the source was at the position $(x_0,\ y_0)$ along the orbit, travels away ballistically from the source and at time $t > \tau$ reaches a position (x, y, z) given by

$$x(t,\tau) = x_0 + (t-\tau)\, v_x(\tau),$$

$$y(t,\tau) = y_0 + (t-\tau)\, v_y(\tau),$$

$$z(t,\tau) = (t-\tau)\, v_j\,. \tag{8}$$

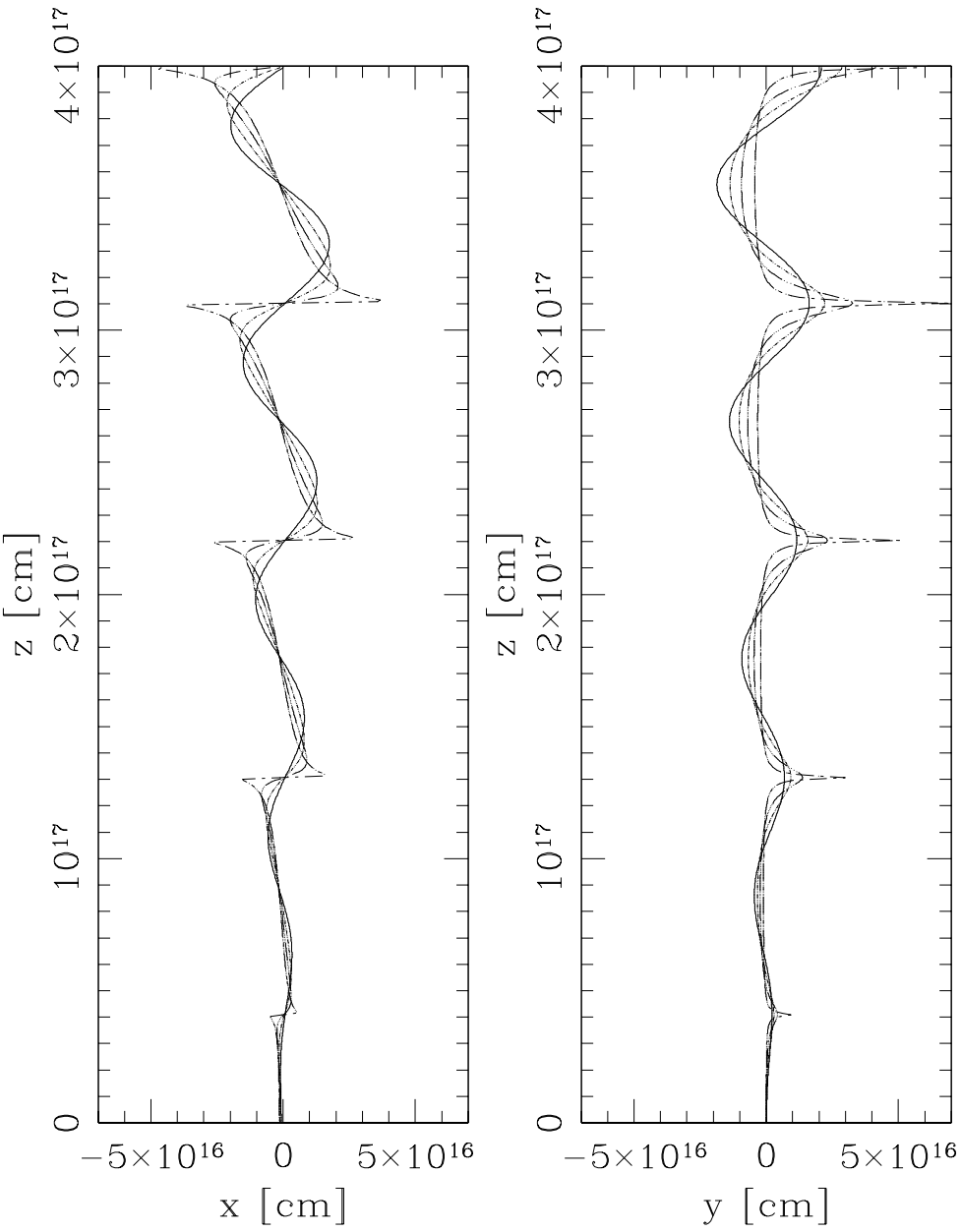

Fig. 1. Projection on the xz- (left) and yz-plane (right) of the ballistic jet solutions (Eq. 8) for a source in elliptical orbits with eccentricities e =0 (circular orbit, resulting in the curves with smooth, symmetric excursions to both sides of the z-axis), 0.3, 0.6, and 0.9 (resulting in the curve with almost-discontinuous jumps in the xz-projection, and in the curve with "spikes" in the $+y$-direction in the yz-direction). The curves correspond to a jet ejected (in z direction) with velocity $v_j = 200$ km s^{-1} by a star with an orbital period of 142 yr and a major semiaxis $a = 50$ AU. The discussion of the curves are given in the text (§ 2). The x, y, and z-axes are labeled in cm.

Figure 1 shows the projection on the xz- (left) and yz-plane (right) of the trajectories of the jets ejected from a star in elliptical orbits. In our examples, we have adopted the orbital parameters $a = 50$ AU, $w = 1.4{\times}10^{-9}$ s^{-1} (corresponding to an orbital period of 143 yr), $e =$ (0.0, 0.3, 0.6, and 0.9) and $v_j = 200$ km s^{-1}. The results shown correspond to a time $t = 635$ yr. In agreement with Masciadri & Raga (2002), for circular orbits the locus of the jet beam shows a series of smooth excursions to both sides of the z-axis, with increasing amplitudes for larger distances from the source.

For increasing values of the ellipticity e, in the xz-projection (see Fig. 1, left) the locus of the jet

beam develops smooth regions (oblique to the z-axis) joined by more sudden "jumps" which join the extremes of the smooth regions. In this xz-projection, the maximum excursions to both sides of the z-axis have the same magnitude.

A different kind of morphology is seen in the yz-projection (Fig. 1, right). In this plane, for increasing values of e the locus of the jet beam develops smooth segments which are approximately parallel to the z-axis, separated by "spikes" which extend away from the axis in the positive y-direction. These spikes are the result of the successive passages of the source through the periastron of the orbit (at $y = 0$), in which the orbital velocity has its highest value and is directed in the positive y-direction.

The curves presented in Fig. 1 correspond to the ballistic jet solution given by Eq. (8). These curves would correspond to a hypersonic jet with a very high jet-to-environment density ratio, so that the interaction between the jet and the ambient medium does not produce substantial deviations from a ballistic motion.

In a real situation with a finite jet-to-environment density ratio, one might expect substantial effects from the environmental drag, particularly in regions with features such as the "spikes" seen in the yz-projections of the high e curves (see above and Fig. 1). As these spikes are produced during the short duration, high velocity periastron passages of the orbital motion of the source, they contain only a small amount of mass and momentum, and they are therefore likely to slow down in a considerable way as a result of the environmental drag. This type of effect is illustrated in the following section, in which we show a comparison between the ballistic model and a simulation with the full, 3D gasdynamic equations.

3. NUMERICAL SIMULATION

In this section we present an illustration of the properties of an "orbiting jet" model computed with the full, 3D gasdynamic equations. We carry out the numerical simulation with the "yguazú-a" adaptive grid code (described in detail by Raga, Navarro-González & Villagrán-Muniz 2000), which integrates the 3D (or 2D) radiative gasdynamic equations together with a system of rate equations following the non-equilibrium ionization state of the gas. We have integrated rate equations for the species H I, H II, C II, C III, C IV, O I, O II, O III, O IV, S II, and S III, with the elemental abundances, rate coefficients and cooling rates described in detail by Raga et al. (2002).

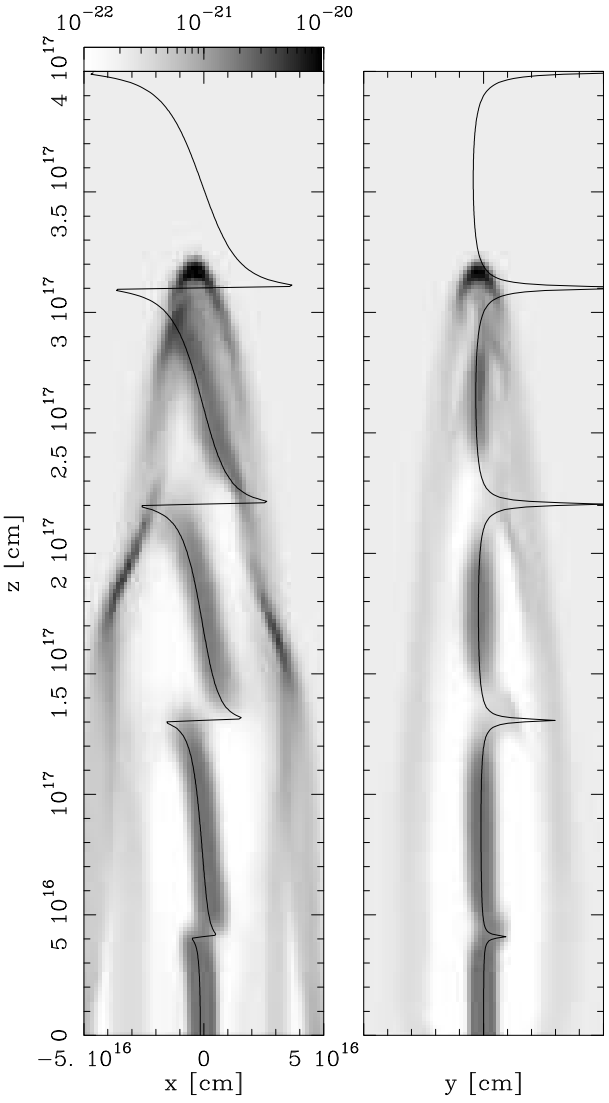

Fig. 2. Density stratifications on the xz- (left) and yz-plane (right) after a $t = 640$ yr time integration. The solid lines correspond to the analytical solutions of the ballistic jet model (with $e = 0.9$) presented in Fig. 1 (also see § 2). A comparison of the numerical simulations with the analytical model is discussed in the text (§ 3). The density stratification is depicted with the logarithmic greyscale shown (in g cm^{-3}) by the bar at the top of the left plot. The x, y, and z-axes are labeled in cm.

The model has been chosen as follows. For the source, we choose an orbit with high eccentricity $e = 0.9$ and major semiaxis $a = 50$ AU. Such an orbit has a velocity $v_p = 45$ km s^{-1} at periastron. We assume that the orbit lies on the xy-plane, and the integration is started with the star at periastron on the x-axis (and moving in the positive y-direction).

For the jet, we choose a (constant) ejection velocity $v_j = 200$ km s^{-1}, density $n_j = 1000$ cm^{-3} and

temperature $T_j = 1000$ K, and a $r_j = 5 \times 10^{15}$ cm initial radius. The surrounding environment is homogeneous, with a density $n_{env} = 100$ cm^{-3} and temperature $T_{env} = 1000$ K. Both the jet and the environment are initially neutral, except for C and S which are singly ionized.

The computation is carried out on a 4-level, binary adaptive grid with a maximum resolution of 1.56×10^{15} cm (along the three axes), and a spatial extent of $(1, 1, 4) \times 10^{17}$ cm along the x, y, and z axes, respectively. The orbit of the jet source is assumed to lie on the xy-plane, with the focus (close to periastron) of the elliptical orbit placed in the middle of this plane. The jet is injected in a circular aperture (of radius $r_j = 5 \times 10^{15}$ cm, see above), which orbits around the focus of the ellipse. The jet material is given a $v_j = 200$ km s^{-1} velocity along the z-axis (see above), as well as the time-dependent velocities $v_x(\tau)$ and $v_y(\tau)$ (see Eq. 5) resulting from the orbital motion of the source. Even though this rather low spatial resolution simulation does resolve neither the jet diameter nor the post-shock cooling distances in an appropriate way, we still expect it to describe the general dynamical properties of the flow in an approximate way.

Figure 2 shows the density stratifications on the xz- and yz mid-planes of the simulation, after a $t = 640$ yr time-integration. Superimposed on the density stratifications, we show the locus of the jet beam predicted by the analytic, ballistic model (see § 2) for the same orbital and flow parameters.

We first note that by this time ($t = 640$ yr, see Fig. 2) the ballistic model has reached a distance $z \approx 4 \times 10^{17}$ along the z-axis, while the numerical model has only reached a $z \approx 3.3 \times 10^{17}$ cm. This effect is due to the presence of the environment, which slows down the propagation of the head of the jet in the numerical model.

In the xz-cut (see Fig. 2), we see that upstream of the jet head the numerical model has a jet beam which mostly coincides with the ballistic model. The main deviations (in this region) between the numerical and ballistic model occur at $z \approx 2.4 \times 10^{17}$ cm, where the maximum excursions away from the z-axis are truncated in the numerical model. This truncation occurs because in this region the jet beam touches the leading bow shock, and interacts directly with the surrounding environment, leading to the production of "swept back" bow shock wing-like structures.

Such an effect is much more clearly seen in the yz-cut (see Fig. 2). In this cut the ballistic model shows extreme excursions in the positive y-direction, resulting from the fast, periastron passages of the source at $y = 0$ (in which the orbital velocity is directed in the positive y-direction, see above). These extreme excursions are not seen in the numerical model, which instead shows extended, swept-back wings (extending to the right hand side of the jet beam) that result from the interaction with the surrounding environment of the material with large initial v_y.

This is of course only an example of the possible configurations that can be adopted by a non-ballistic model of a jet from a source moving in an elliptical orbit. The characteristics of the flow will of course depend not only on the jet velocity and the properties of the orbit, but also on the jet-to-environment density ratio, which will determine the magnitude of the deviations of the flow from the ballistic motion.

4. OBSERVATIONAL PROPERTIES

In Figure 3 we show the Hα intensity maps predicted from our numerical simulation for a $t = 640$ yr integration time. The two maps of this figure have been calculated assuming that the y (left) and x-axis (right) are parallel to the line of sight (respectively). It is clear that very different morphologies are predicted for the two orientations of the flow with respect to the observer.

For the observer along the y-axis (left, Fig. 3), we see the emission from the leading head of the jet and from the extended bow shock wings. These wings show bright "shoulders" at each side of the flow axis, which are produced by the side-to-side excursions of the jet beam (resulting from the orbital motion of the source, see Fig. 1). The central region (containing the jet beam itself) does not show bright Hα emission.

For the case of an observer along the x-axis (right, Fig. 3), the emission is much more collimated. The central region now has bright Hα emission. However, this emission does not come from the jet beam itself, but from the two "shoulders" of the bow shock extending away from the outflow axis in the $\pm x$ direction (see the left hand plots of Figs. 2 and 3). The bow shock wings do not show comparable features in the yz-projection (right, Fig. 3). However, the successive periastron passages of the orbital motion of the source results in the production of swept-back features extending away from the outflow axis in the positive y-direction.

5. CONCLUSIONS

We have computed ballistic analytic models (§ 2) and a 3D numerical simulation (§§ 3, 4) of a jet ejected from a source moving in an elliptical orbit

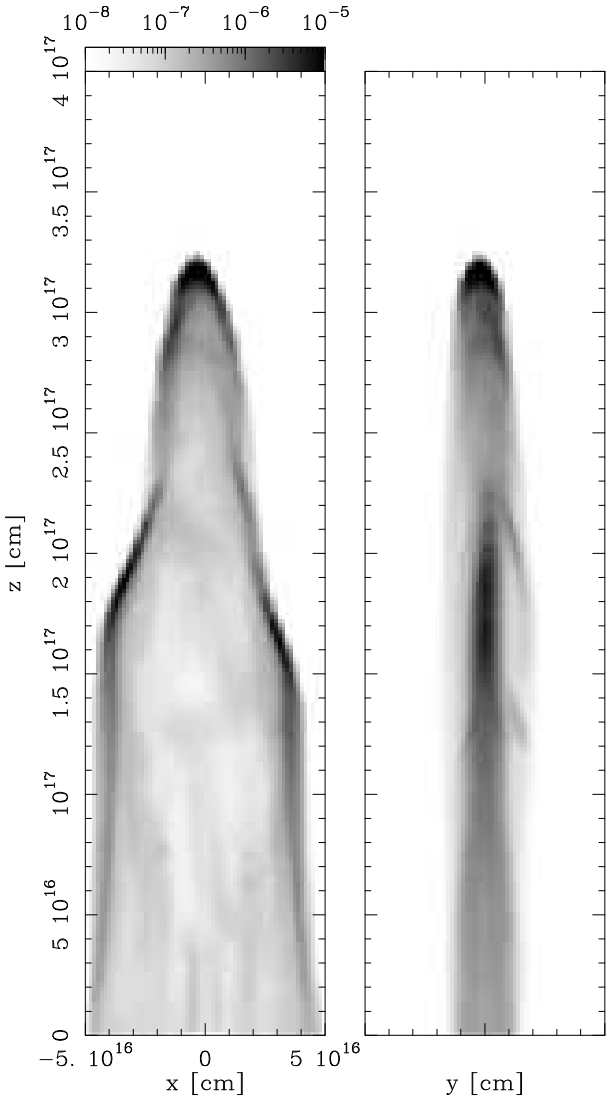

Fig. 3. Hα intensity maps predicted from the numerical simulations presented in Fig. 2 (also see § 3) for a $t = 640$ yr integration time. For the two maps we have assumed that the y- (left) and the x-axis (right) are parallel to the line of sight, respectively (see § 4). The intensity maps are depicted with the logarithmic greyscale shown (in erg s^{-1} cm^{-2} sterad^{-1}) by the bar at the top of the left plot. The x, y and z-axes are labeled in cm.

around a stellar companion. We have assumed that the jet is ejected with a time-independent density and velocity (on which we superimpose the orbital motion), with an initial direction (measured in a frame moving with the source) perpendicular to the orbital plane.

As expected, we find that the projections of the jet locus on a plane parallel to the major axis of the orbital motion (the xz-plane of Figs. 1–3) show symmetric excursions to both sides of the outflow axis. We also find that the projections on a plane parallel to the minor axis of the orbital motion (the yz-plane of Figs. 1–3) show highly asymmetric excursions, which result from the asymmetries between the high velocity, periastron passage and the low velocity, apoastron passage (both occurring at $y = 0$, but with oppositely directed velocities).

From our analytic, ballistic jet model we therefore conclude that a wide range of possible morphologies could be produced in jets from orbiting sources, depending on the ellipticity e of the orbit, and also on the orientation angle of the orbit with respect to the observer. These morphologies include (see Fig. 1):

- smooth, symmetric, side-to-side excursions of the jet beam (as obtained for $e = 0$),
- smooth jet beam segments which are oblique to the outflow axis and are joined by "jumps" in the locus of the jet beam (as seen on the xz-projections of the high e solutions),
- jet beam segments parallel to the outflow axis, separated by "spikes" extending to one side of the axis (as seen on the yz-projections of the high e solutions).

As shown by the numerical simulation of § 3, some of the features of the ballistic solution might be substantially distorted as a result of the interaction with the surrounding environment.

In the Hα intensity maps predicted from our numerical simulation (see § 4 and Fig. 3) we do not see the ballistic sections of the jet beam in a direct way. The Hα emission is dominated by the shocks generated in the interaction between the jet beam and the surrounding environment, so that we see the wings of the leading bow shock (distorted by the side-to-side excursions of the jet beam) and the swept-back jet beam sections (which result from the interactions with the environment of the "spikes" produced at the periastron passages).

This kind of swept-back structures on one side of the outflow (right, Fig. 3) are reminiscent of some HH jets with strong side-to-side asymetries. The best example of this kind of morphology is provided by HH 46/47 (Heathcote et al. 1996), which shows a series of swept-back filaments extending away to the south of the jet.

It is believed that in many HH jets the ejection velocity varies with time, leading to the production of trains of working surfaces which excite emission along the jet beam. Such a process would allow us to see the jet beam material in a direct way, as well as the "kinks" and side-to-side asymetries predicted

by the ballistic model (see Fig. 1) in a direct way. Interestingly, Reipurth et al. (2002) have found a "kink" in the beam of the HH 34 jet, which they suggest might be the result of a periastron passage of the outflow source in a highly eccentric orbit. This object therefore is possibly the best candidate for a direct application of our models.

Of course, our models of a jet from an elliptically orbiting source have the problem that even though the jet parameters (i.e., jet velocity, density, radius, and environmental properties) are constrained by the observations of the HH jets, the orbital parameters (orbital period, major axis, period, and orientation of the orbit with respect to the observer) are mostly unconstrained. This lack of constraint allows a wide variety of different flow morphologies, which can only be used as an illustration of the possible observational properties of such flows, rather than as models for particular HH jets.

This situation might change in the near future, as recent proper motion determinations (carried out with radio interferometers) are starting to provide direct constraints on the orbits of binary or multiple young stars (Loinard et al. 2002; Rodríguez et at. 2003; Loinard, Rodríguez, & Rodríguez 2003). With time-baselines of a few more years, this kind of study will soon yield the full orbital parameters of at least some sources of HH outflows, providing the information necessary for applying the models described in the present paper to specific objects.

This work was supported by the CONACyT grants 36572-E and 41320, and the DGAPA (UNAM) grant IN 112602. We thank Israel Díaz for maintaining and supporting our multiprocesor Linux server, where we have carried out our numerical simulations.

REFERENCES

Ferreira, J. 2002, Proceedings of Star Formation and the Physics of Young Stars, eds. J. Bouvier & J.-P. Zahn (Aussois, France: EDP Sciences EAS Publication Series), Vol. 3, 229

Goldstein, H. 1980, Classical Mechanics (Massachusetts: Addison Wesley)

Heathcote, S., Morse, J. A., Hartigan, P., Reipurth, B., Schwartz, R. D., Bally, J., & Stone, J. M. 1996, AJ, 112, 1141

Loinard, L., Rodríguez, L. F., D'Alessio, P., Wilner, D. J., & Ho, P. T. P. 2002, ApJ, 581, L109

Loinard, L., Rodríguez, L. F., & Rodríguez, M. I. 2003, ApJ, 587, L47

Masciadri, E., de Gouveia Dal Pino, E. M., Raga, A. C., & Noriega-Crespo, A. 2002, ApJ, 580, 950

Masciadri, E., & Raga, A. C. 2002, ApJ, 568, 733

Raga, A. C., Cantó, J., & Biro, S. 1993, MNRAS, 260, 163

Raga, A. C., de Gouveia dal Pino, E. M., Noriega-Crespo, A., Mininni, P., & Velázquez, P. F. 2002, A&A, 392, 267

Raga, A. C., Navarro-González, R., & Villagrán-Muniz, M. 2000, RevMexAA, 36, 67

Reipurth, B. 2000, AJ, 120, 3177

Reipurth, B., Heathcote, S., Morse, J., Hartigan, P., & Bally, J. 2002, AJ, 123, 362

Rodríguez, L. F., Curiel, S., Cantó, J., Loinard, L., Raga, A. C., & Torrelles, J. M. 2003, ApJ, 583, 330

Terquem, C., Eislöffel, J. Papaloizou, J. C. B., & Nelson, R. P. 1999, ApJ, 512, L131

Völker, R., Smith, M. D., Suttner, G., & Yorke, H. W. 1999, A&A, 343, 953

Ricardo F. González and Alejandro C. Raga: Instituto de Ciencias Nucleares, UNAM, Apdo. Postal 70-543, 04510 México, D. F., México (raga;ricardog@nuclecu.unam.mx).